Chinese Physics C Vol. 50, No. 10 (2026) 105105

Hernquist dark matter halo: new self-consistent black hole exact solution of einstein equation, optical and ringing signatures and thermodynamics

David Senjaya[†]

Department of Physics, Faculty of Science, Mahidol University, Bangkok 10400, Thailand

Abstract: Recent advances in black hole imaging and gravitational-wave observations have intensified interest in understanding how realistic astrophysical environments modify black hole spacetimes. In this work, we construct an exact, static, spherically symmetric black hole solution embedded within a Hernquist dark matter halo by solving the full Einstein field equations. We subsequently investigate how the surrounding halo reshapes the geometry and observable properties of the black hole. Through an analysis of null geodesics, we demonstrate that the dark matter distribution significantly alters photon trajectories, displaces circular photon orbits, and distorts the associated gravitational lensing structure. Using the Lyapunov exponent of unstable null geodesics, we further determine the behavior of massless quasinormal modes in the eikonal regime, revealing explicit halo-induced corrections to the oscillation frequencies and damping rates. We also examine the thermodynamic behavior of the black hole–halo configuration by evaluating the conserved mass, temperature, entropy, heat capacity, and Gibbs free energy, thereby enabling a detailed analysis of local and global thermal stability. Our results reveal that the Hernquist dark matter halo reduces both the photon-sphere radius and the apparent shadow size, while substantially enlarging the region of thermodynamic stability and producing nontrivial phase structures absent from the Schwarzschild vacuum spacetime. These findings demonstrate that astrophysical dark matter environments can leave measurable imprints on both optical and thermodynamic observables, offering a potential avenue for probing halo-induced gravitational effects around black holes.

Keywords: Hernquist halo, black hole chemistry, null geodesic, lyapunov exponent, quasinormal modes

DOI: 10.1088/1674-1137/ae8824 **CSTR:** 32044.14.ChinesePhysicsC.50105105

I. INTRODUCTION

In recent years, black holes embedded in astrophysically realistic dark matter environments have attracted considerable attention as promising astrophysical systems for exploring gravitational physics beyond idealized vacuum spacetimes. In particular, black hole solutions surrounded by Dehnen-type double power-law dark matter halos have been extensively investigated across various halo configurations, including $(1,4,0)$ [1], $\left(1,4,\frac{1}{2}\right)$ [2], $(1,4,1)$ [3], $\left(1,4,\frac{3}{2}\right)$ [4], $(1,4,2)$ [5], and $\left(1,4,\frac{5}{2}\right)$ [6, 7]. These studies have revealed that the surrounding dark matter distribution induces significant and nontrivial physical effects, ranging from modifications of black hole thermodynamics and phase structure to observable changes in gravitational lensing and shadow formation.

This growing interest has been driven by remarkable observational advances in astrophysics. The direct detection of gravitational waves by the LIGO/Virgo Collaboration and the imaging of black hole shadows by the Event Horizon Telescope have provided compelling confirmation of General Relativity in the strong-gravity regime [8, 9]. Nevertheless, on galactic and cosmological scales, baryonic matter alone remains insufficient to explain the observed dynamics of galaxies, particularly their nearly flat rotation curves. This discrepancy has led to the dark matter paradigm, which posits that dark matter constitutes the dominant mass component of galaxies. Observational evidence suggests that baryonic matter contributes only a small fraction of the total galactic mass, whereas dark matter accounts for nearly 90% of the mass inferred from stellar dynamics. During the early stages of cosmic evolution, dark matter is thought to have been more concentrated near galactic centers, thereby facilitating galactic structure and star formation, before gradually evolving into extended halo distributions. Furthermore, observations indicate that most massive spiral and ellipt-

Received 9 June 2026; Accepted 8 July 2026; Accepted manuscript online 9 July 2026

[†] E-mail: davidsenjaya@protonmail.com;

ical galaxies harbor supermassive black holes embedded within these dense dark matter halos [10]. These considerations render black holes in dark matter environments crucial astrophysical laboratories for investigating gravitational phenomena, galactic dynamics, and potential signatures of new physics beyond General Relativity.

Among the various phenomenological models used to characterize dark matter distributions, the double power-law family provides a particularly versatile analytic framework for modeling both stellar systems and galactic halos [11, 12]. The general density profile is given by

$$\rho(r) = \rho_0 \left(\frac{r}{r_0}\right)^{-\gamma} \left[1 + \left(\frac{r}{r_0}\right)^{\alpha}\right]^{\frac{\gamma-\beta}{\alpha}}, \tag{1}$$

where the parameters (α,β,γ) characterize the sharpness of the transition region, the asymptotic outer slope, and the inner logarithmic behavior of the density profile, respectively. Specific choices of these parameters reproduce several widely studied dark matter halo models. For instance, cuspy profiles include the Navarro–Frenk–White (NFW) model $(1,3,1)$ and the Hernquist profile $(1,4,1)$, whereas cored distributions include the pseudo-isothermal profile $(2,2,0)$, the cored Plummer profile $(2,4,0)$ [13], the cored NFW profile [14], and the Burkert profile $\left(\frac{3}{2},3,0\right)$ [15].

Recently, several studies have investigated black holes immersed in Hernquist dark matter halos. An effective Schwarzschild–Hernquist spacetime was constructed in Ref. [16] using the phenomenological approach of Ref. [17]; however, this metric was not derived as an exact solution of the Einstein field equations. Subsequently, self-consistent Hernquist black hole solutions obtained directly from the Einstein equations were reported [18?, 19]. These works focused primarily on specific aspects of the spacetime, such as null geodesics and thermodynamic properties. Nevertheless, a comprehensive investigation combining optical properties, eikonal quasinormal modes via the Lyapunov exponent, and the detailed thermodynamic phase structure has not yet been undertaken.

Motivated by these developments, we construct an exact black hole solution embedded in a Hernquist dark matter halo by solving the full Einstein field equations self-consistently. Building upon this exact solution, we perform a unified analysis of its optical, dynamical, and thermodynamic properties. Specifically, we investigate null geodesics, gravitational lensing, and unstable photon orbits; the associated Lyapunov exponent and eikonal quasinormal modes; and the conserved mass, entropy, temperature, heat capacity, Gibbs free energy, and thermal phase structure.

In the present work, we consider the Hernquist profile, which corresponds to the parameter choice

$$(\alpha,\beta,\gamma) = (1,4,1), \tag{2}$$

for which the dark matter density distribution takes the form

$$\rho_{\rm DM}(r) = \rho_0 \left(\frac{r}{r_0}\right)^{-1} \left(1 + \frac{r}{r_0}\right)^{-3}, \tag{3}$$

where ρ_0 denotes the characteristic density and r_0 represents the characteristic halo radius.

The Hernquist profile exhibits a cuspy inner region, $\rho \propto r^{-1}$ for $r \ll r_0$, whereas at large distances the density decreases as $\rho \propto r^{-4}$ for $r \gg r_0$. Owing to this steep asymptotic decay, the cumulative mass approaches a finite value as $r \to \infty$, rendering the total halo mass well-defined. This feature distinguishes the Hernquist profile from several other phenomenological dark matter models in which the total mass diverges logarithmically at large radii. Furthermore, the Hernquist profile has been widely employed in galactic dynamics because it provides an analytic description that successfully captures the mass distribution of elliptical galaxies and dark matter halos while remaining mathematically tractable.

Understanding the influence of dark matter halos on black holes is essential for developing realistic descriptions of galactic dynamics and strongly gravitating systems. In astrophysical environments, supermassive black holes residing at galactic centers are expected to be surrounded by extended dark matter halos, whose properties are intimately connected to observed galactic dynamics, including the nearly flat behavior of galactic rotation curves. Consequently, black hole–dark matter configurations provide a natural setting to explore the interplay between compact gravitating objects and their large-scale environments. Such studies may offer valuable insights into the relationship between black hole physics, dark matter phenomenology, and the mechanisms governing galaxy formation and evolution.

The thermodynamic behavior of black holes provides an additional important perspective for understanding these systems. Since the pioneering works of Bekenstein and Hawking, black holes have been recognized as thermodynamic objects possessing an entropy proportional to the area of the event horizon, which obeys the irreversible area law in classical processes [20]. At the macroscopic level, stationary black holes are remarkably simple, completely characterized by their mass M, electric charge Q, and angular momentum J [21–25]. Together with the Hawking temperature, these quantities form the basis of black hole thermodynamics and are formalized in the four laws established in the 1970s [20]. More recently, the development of black hole chemistry has substantially enriched this framework by interpreting the cosmological constant as a thermodynamic pressure, thereby uncovering intricate phase structures and deep analogies between black holes and ordinary thermodynamic systems [26, 27].

The present paper is organized as follows. We first construct an exact static and spherically symmetric black hole solution immersed in a Hernquist dark matter halo by solving the Einstein field equations consistent with the underlying matter distribution. We then investigate the properties of null geodesics, analyzing the associated photon trajectories and orbital structure. We further examine the stability of unstable circular null orbits via the Lyapunov exponent, which allows us to determine the corresponding quasinormal modes in the eikonal regime. Finally, we study the thermodynamic properties of the black hole–dark matter system and discuss the influence of the Hernquist halo on its thermal stability and phase behavior. Overall, our analysis demonstrates that the surrounding dark matter halo can significantly modify both the dynamical and thermodynamic characteristics of the black hole spacetime.

II. BLACK HOLE CONSTRUCTION

To investigate the gravitational influence of a Hernquist dark matter halo on a central compact object, we construct a static, spherically symmetric black hole solution embedded within this dark matter distribution. The spacetime geometry is described by the metric ansatz

$$\mathrm{d}s^2 = -h(r)\mathrm{d}t^2 + \frac{\mathrm{d}r^2}{h(r)} + r^2\left(\mathrm{d}\theta^2 + \sin^2\theta\mathrm{d}\phi^2\right), \tag{4}$$

where the metric function $h(r)$ encodes the combined gravitational effects of the black hole and the dark matter halo.

The energy–momentum tensor is assumed to take the anisotropic form

$$T^{\mu}_{\ \nu} = \mathrm{diag}\left[-\rho_{\mathrm{DM}}(r), p_r(r), p_t(r), p_t(r)\right], \tag{5}$$

where $\rho_{\mathrm{DM}}(r)$ represents the Hernquist dark matter density profile, and $p_r(r)$ and $p_t(r)$ denote the radial and tangential pressures, respectively. These quantities are determined self-consistently from the Einstein field equations.

For the metric ansatz (4), the Einstein equations reduce to

- **Temporal component:**

$$G_{tt} = -\frac{h(r)}{r^2}\left[rh'(r) + h(r) - 1\right] = 8\pi h(r)\rho_{\mathrm{DM}}(r), \tag{6}$$

- **Radial component:**

$$G_{rr} = \frac{1}{r^2 h(r)}\left[rh'(r) + h(r) - 1\right] = 8\pi\frac{p_r(r)}{h(r)}, \tag{7}$$

- **Angular components:**

$$G_{\theta\theta} = \frac{G_{\phi\phi}}{\sin^2\theta} = \frac{r^2}{2}h''(r) + rh'(r) = 8\pi r^2 p_t(r). \tag{8}$$

Here, primes denote derivatives with respect to the radial coordinate r. The temporal and radial equations differ only by an overall sign, thereby implying the relation

$$p_r(r) = -\rho_{\mathrm{DM}}(r), \tag{9}$$

which is a generic feature of static, spherically symmetric anisotropic matter distributions in Schwarzschild-like coordinates.

Substituting the Hernquist density profile

$$\rho_{\mathrm{DM}}(r) = \rho_0\left(\frac{r}{r_0}\right)^{-1}\left(1 + \frac{r}{r_0}\right)^{-3}, \tag{10}$$

into the temporal Einstein equation yields

$$\frac{\mathrm{d}}{\mathrm{d}r}\left[r(1 - h(r))\right] = -8\pi r^2\rho_{\mathrm{DM}}(r). \tag{11}$$

Integrating both sides with respect to r, we obtain

$$r(1 - h(r)) = C - 8\pi\int r^2\rho_{\mathrm{DM}}(r)\,\mathrm{d}r, \tag{12}$$

where C is an integration constant. Imposing the Schwarzschild limit in the absence of dark matter fixes this constant as

$$C = r_s = 2M. \tag{13}$$

Here, M denotes the black hole mass. Consequently, the metric function can be expressed as

$$h(r) = 1 - \frac{r_s}{r} - \frac{8\pi}{r}\int_0^r \rho_{\mathrm{DM}}(r')\,r'^2\,\mathrm{d}r'. \tag{14}$$

Substituting the explicit form of the Hernquist profile yields

$$\int_0^r \rho_{\mathrm{DM}}(r')\,r'^2\,\mathrm{d}r' = \rho_0 r_0^3\int_0^r \frac{r'}{(r' + r_0)^3}\,\mathrm{d}r'. \tag{15}$$

The integral can be evaluated analytically as

$$\int \frac{r}{(r+r_0)^3}\,\mathrm{d}r = \int \left[\frac{1}{(r+r_0)^2} - \frac{r_0}{(r+r_0)^3}\right]\mathrm{d}r = -\frac{1}{r+r_0} + \frac{r_0}{2(r+r_0)^2}. \tag{16}$$

Evaluating between 0 and r yields

$$\int_0^r \rho_{\mathrm{DM}}(r')\,r'^2\,\mathrm{d}r' = \frac{\rho_0 r_0^3 r^2}{2(r+r_0)^2}. \tag{17}$$

Thus, the complete static and spherically symmetric black-hole solution surrounded by a Hernquist dark matter halo is given by

$$\mathrm{d}s^2 = -h(r)\mathrm{d}t^2 + \frac{\mathrm{d}r^2}{h(r)} + r^2\mathrm{d}\Omega_2^2, \tag{18}$$

$$h(r) = 1 - \frac{r_s}{r} - \frac{4\pi\rho_0 r_0^3 r}{(r+r_0)^2}. \tag{19}$$

The first contribution to the metric function corresponds to the standard Schwarzschild geometry generated by the central black hole, while the final term represents the gravitational correction induced by the surrounding Hernquist dark matter halo.

III. NULL GEODESICS

We analyze the propagation of photons in the spacetime of a Schwarzschild black hole immersed in a Hernquist dark matter halo, which is described by the metric (19). The motion of massless particles is governed by the Lagrangian

$$\mathcal{L}(x^\mu,\dot{x}^\mu) = \frac{1}{2}g_{\mu\nu}\dot{x}^\mu\dot{x}^\nu = \frac{1}{2}\left[-h(r)\dot{t}^2 + \frac{\dot{r}^2}{h(r)} + r^2\dot{\theta}^2 + r^2\sin^2\theta\,\dot{\phi}^2\right] = 0, \tag{20}$$

where the null condition $\mathcal{L}=0$ signifies the massless nature of photon trajectories.

Since the metric is independent of the coordinates t and ϕ, the corresponding conjugate momenta are conserved along the geodesics. These conserved quantities correspond to the photon energy E and angular momentum L, respectively,

$$p_t = \frac{\partial\mathcal{L}}{\partial\dot{t}} = -h(r)\dot{t} = -E, \tag{21}$$

$$p_\phi = \frac{\partial\mathcal{L}}{\partial\dot{\phi}} = r^2\sin^2\theta\,\dot{\phi} = L. \tag{22}$$

By exploiting the spherical symmetry of the spacetime, photon motion can be confined, without loss of generality, to the equatorial plane,

$$\theta = \frac{\pi}{2}, \tag{23}$$

which reduces the Lagrangian to

$$\mathcal{L}(r,\dot{t},\dot{r},\dot{\phi}) = \frac{1}{2}\left[-h(r)\dot{t}^2 + \frac{\dot{r}^2}{h(r)} + r^2\dot{\phi}^2\right] = \frac{1}{2}\left[-\frac{E^2}{h(r)} + \frac{\dot{r}^2}{h(r)} + \frac{L^2}{r^2}\right] = 0. \tag{24}$$

The above equation governs the dynamics of photons in the effective gravitational field generated by both the black hole and the surrounding dark matter halo. Consequently, it serves as the basis for investigating circular photon orbits, gravitational lensing, and shadow formation.

From Eq. (24), the radial equation of motion is expressed as

$$\dot{r}^2 + \frac{L^2}{r^2}h(r) = E^2, \tag{25}$$

where the first term represents the radial kinetic component, while the second denotes the effective potential governing photon motion. Introducing the impact parameter

$$b = \frac{L}{E}, \tag{26}$$

the effective potential becomes

$$\frac{V_{\mathrm{eff}}}{E^2} = \frac{b^2}{r^2}h(r) = \frac{b^2}{r^2}\left[1 - \frac{r_s}{r} - \frac{4\pi\rho_0 r_0^3 r}{(r+r_0)^2}\right]. \tag{27}$$

Figure 1 illustrates the effective potential V_{eff}/E^2 for photon motion around a Schwarzschild black hole surrounded by a Hernquist dark matter halo. The curves correspond to varying combinations of the halo parameters ρ_0 and r_0 and the photon impact parameter b. The peak of the effective potential determines the photon sphere radius, which corresponds to unstable circular null geodesics. Variations in the halo parameters alter both the height and position of the potential barrier, demonstrating that the surrounding dark matter distribution significantly affects photon trajectories and the optical structure of the spacetime.

We now examine circular photon motion in the spacetime of a Schwarzschild black hole surrounded by a Hernquist dark matter halo. Circular null geodesics play a fundamental role in determining the optical appearance of

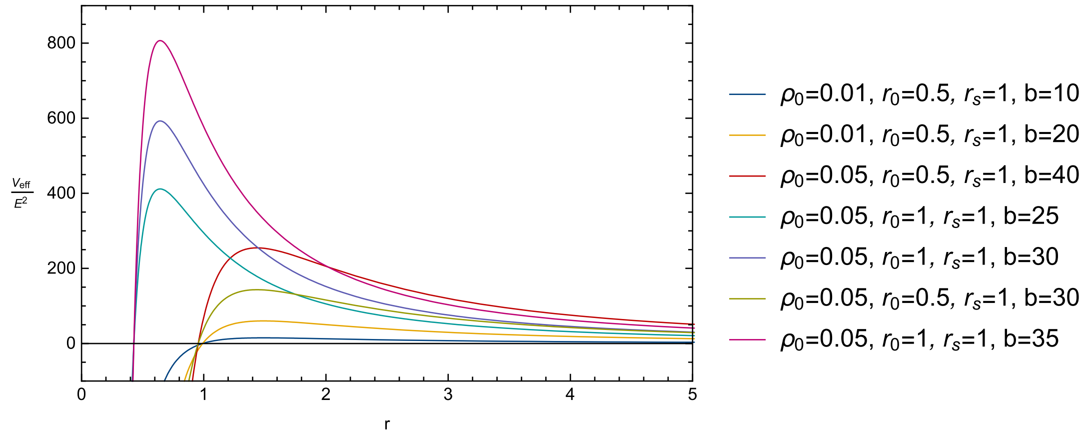

Fig. 1. (color online) Effective potential $V_{\rm eff}/E^2$ for different values of the halo parameters and the impact parameter.

the spacetime. They govern the formation of the photon sphere and strongly influence gravitational lensing and black hole shadow observables. In the equatorial plane, circular photon orbits satisfy the conditions

$$\dot{r}=0, \qquad \frac{{\rm d}V_{\rm eff}}{{\rm d}r}=0, \tag{28}$$

where the second condition ensures that the radial force vanishes at the orbital radius.

From the radial equation of motion (25), the condition for circular photon motion becomes

$$\frac{V_{\rm eff}}{E^2}=\frac{b^2}{r^2}\left[1-\frac{r_s}{r}-\frac{4\pi\rho_0 r_0^3 r}{(r+r_0)^2}\right]=1. \tag{29}$$

The radius of the circular photon orbit is determined by the extremum of the effective potential. Differentiating $V_{\rm eff}$ with respect to r yields

$$\frac{{\rm d}V_{\rm eff}}{{\rm d}r}=\frac{b^2}{r^4}\left[-2r+3r_s+\frac{4\pi\rho_0 r_0^3 r^2(r-r_0)}{(r+r_0)^3}\right]=0. \tag{30}$$

To analyze photon trajectories explicitly, we re-express the radial equation in terms of the azimuthal coordinate ϕ. Using

$$\dot{r}=\frac{{\rm d}r}{{\rm d}\phi}\dot{\phi}, \tag{31}$$

along with the impact parameter definition

$$b=\frac{L}{E}, \tag{32}$$

the radial equation (25) becomes

$$\begin{aligned}\left(\frac{{\rm d}r}{{\rm d}\phi}\right)^2&=\frac{r^4}{L^2}\left(E^2-\frac{L^2}{r^2}h(r)\right)\\&=\frac{r^4}{b^2}-r^2h(r)=r^2h(r)\left(\frac{r^2}{b^2h(r)}-1\right).\end{aligned} \tag{33}$$

Figure 2 illustrates representative photon trajectories for impact parameters in the range $1\le b\le 10$ for the black hole–dark matter configuration characterized by $r_s=2$, $\rho_0=0.02$, and $r_0=0.4$. The black disk represents the event horizon, while the red dashed circle denotes its boundary at $r=1.995$. The yellow circle at $r=2.993$ indicates the unstable photon sphere, separating captured trajectories from scattered ones.

The figure demonstrates the significant influence of spacetime curvature on photon propagation. Photons with sufficiently small impact parameters are inevitably captured by the black hole, spiraling inward after crossing the photon sphere. Near the critical impact parameter, trajectories undergo large deflections and can orbit the black hole multiple times before escaping or plunging into the horizon. As the impact parameter increases, the deflection angle decreases, and the trajectories tend toward straight-line propagation. These features illustrate how the surrounding Hernquist dark matter halo modifies the optical structure of the spacetime and alters null geodesic behavior relative to the vacuum Schwarzschild case.

A. Black hole shadow

The black hole shadow is determined by unstable circular photon orbits, commonly known as the photon sphere. These null trajectories define the critical boundary separating photons captured by the black hole from those escaping to infinity. For equatorial motion, circular null geodesics satisfy the conditions

$$\frac{{\rm d}r}{{\rm d}\phi}=0, \qquad \frac{{\rm d}^2r}{{\rm d}\phi^2}=0, \tag{34}$$

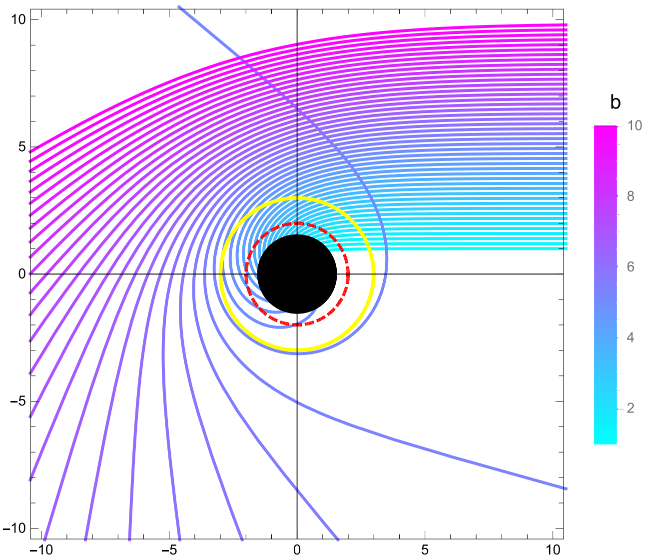

Fig. 2. (color online) Ray-tracing profile of a Schwarzschild black hole embedded in a Hernquist dark matter halo with parameters $r_s = 2$, $\rho_0 = 0.02$, and $r_0 = 0.4$. The black region represents the event horizon, while the yellow circle denotes the unstable photon sphere.

which ensure that both the radial velocity and the radial acceleration vanish.

Application of the radial geodesic equation to the first condition implies

$$\frac{\mathrm{d}r}{\mathrm{d}\phi} = 0 \quad \Rightarrow \quad \frac{r^2}{b^2 h(r)} = 1, \tag{35}$$

while the second condition gives

$$\frac{\mathrm{d}^2 r}{\mathrm{d}\phi^2} = 0 \quad \Rightarrow \quad \frac{\mathrm{d}}{\mathrm{d}r}\left(\frac{r^2}{h(r)}\right) = 0. \tag{36}$$

Equation (36) is equivalent to requiring the effective potential to possess an extremum, which corresponds to the location of the unstable circular photon orbit. This condition can alternatively be expressed in the compact form

$$2rh(r) - r^2 h'(r) = 0. \tag{37}$$

Substituting the explicit metric function into this relation yields the photon sphere equation.

$$2r - 3r_s + \frac{4\pi\rho_0 r_0^3 r^2 (r - r_0)}{(r + r_0)^3} = 0. \tag{38}$$

In the regime where the dark matter contribution is small ($\rho_0 r_0^4 \ll 1$), Eq. (38) can be expanded perturbatively. To leading order, one obtains

$$2r - 3r_s - 4\pi\rho_0 r_0^3 = 0, \tag{39}$$

which yields the approximate photon sphere radius

$$r_{ps} \approx \frac{3}{2} r_s + 2\pi\rho_0 r_0^3. \tag{40}$$

In the absence of dark matter ($\rho_0 = 0$), the above expression reduces to the standard Schwarzschild result.

$$r_{ps} = \frac{3}{2} r_s, \tag{41}$$

which corresponds to the well-known unstable circular null orbit.

The critical impact parameter associated with the photon sphere follows directly from Eq. (35),

$$b_c = \sqrt{\frac{r_{ps}^2}{h(r_{ps})}}. \tag{42}$$

This quantity defines the threshold between captured and scattered photon trajectories. Photons with $b < b_c$ are captured by the black hole after crossing the photon sphere, whereas photons with $b > b_c$ are gravitationally deflected and ultimately escape to infinity. Consequently, the critical impact parameter determines the apparent radius of the black hole shadow for a distant observer.

Following [28], the shadow radius is thus given by

$$R_s = b_c \sqrt{h(r \to \infty)} = \sqrt{\frac{r_{ps}^2}{h(r_{ps})}}. \tag{43}$$

By employing the perturbative expression (40), the shadow radius in the weak dark matter regime becomes

$$R_s \approx \frac{3\sqrt{3}}{2} r_s + 2\sqrt{3}\pi\rho_0 r_0^3. \tag{44}$$

In the vacuum limit, the standard Schwarzschild shadow radius is recovered,

$$R_s = \frac{3\sqrt{3}}{2} r_s, \tag{45}$$

in agreement with the well-known result for Schwarzschild black holes [29].

Figure 3 illustrates the dependence of the shadow radius on the Hernquist dark matter parameters $\{\rho_0, r_0\}$ for a fixed Schwarzschild radius $r_s = 1$. The left panel shows the variation of the photon ring as the dark matter density

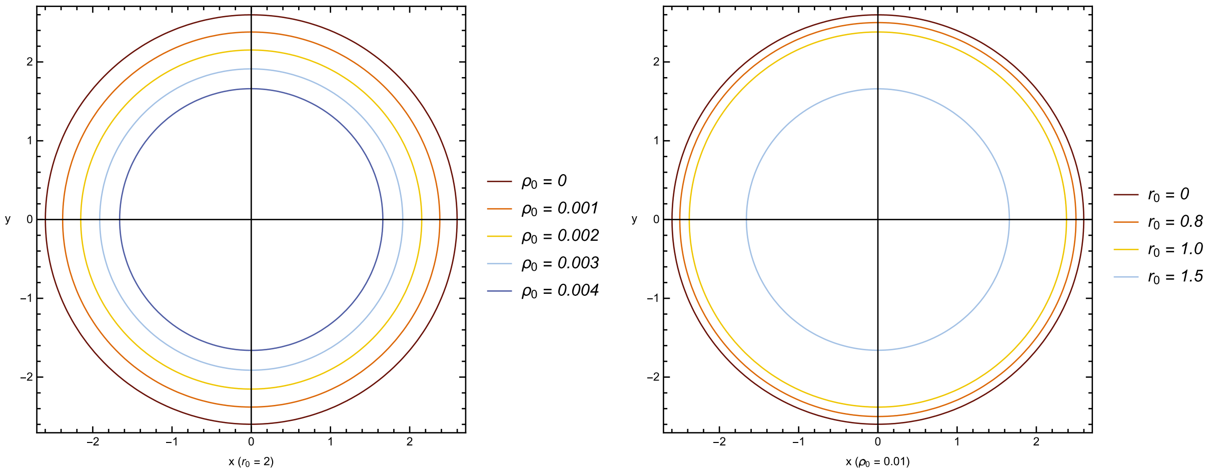

Fig. 3. (color online) Profiles of the shadow radius R_s for various values of the Hernquist dark matter parameters $\{\rho_0, r_0\}$, with a fixed Schwarzschild radius $r_s = 1$.

ρ_0 increases at a fixed $r_0 = 2$, while the right panel displays the effect of varying the halo scale radius r_0 at a fixed $\rho_0 = 0.01$. In both cases, the surrounding dark matter distribution shifts the location of the photon sphere and alters the apparent size of the black hole shadow, demonstrating that the halo environment can leave potentially observable imprints on the optical signatures of black holes.

B. Weak deflection angle

We investigate the weak gravitational lensing produced by a Schwarzschild black hole immersed in a Hernquist dark matter halo. In the weak-field regime, the deflection of light can be analyzed using the Gauss–Bonnet theorem applied to the corresponding optical geometry, following the geometric approach developed by Gibbons and Werner [30, 31]. Unlike the standard geodesic method, this formalism relates the deflection angle to the global curvature properties of the optical manifold, thereby providing an elegant description of gravitational lensing. Alternative approaches based on elliptic integrals and strong-field expansions are discussed in [32, 33].

In the weak deflection limit, the deflection angle α is given by [34]

$$\alpha = \int_0^{\pi} \int_{\frac{b}{\sin\phi}}^{\infty} K \sqrt{g_{\rm opt}}\, \mathrm{d}r\, \mathrm{d}\phi, \tag{46}$$

where K denotes the Gaussian curvature of the optical geometry, and $g_{\rm opt}$ is the determinant of the corresponding two-dimensional optical metric.

For null trajectories, the optical metric corresponding to the spacetime line element (19) can be expressed as

$$\mathrm{d}t^2 = \frac{\mathrm{d}r^2}{h^2(r)} + \frac{r^2}{h(r)}\mathrm{d}\phi^2, \tag{47}$$

from which the determinant follows directly as

$$g_{\rm opt} = \frac{r^2}{h^3(r)}. \tag{48}$$

The Gaussian curvature of the optical manifold is derived from the two-dimensional Ricci scalar associated with the metric (47). A direct computation yields

$$K = \frac{1}{2}\left[\frac{1}{2}(h'(r))^2 - h(r)h''(r)\right]. \tag{49}$$

Substituting the metric function (19) and expanding in the weak dark matter regime to leading order in $\rho_0 r_0^3$, we find that the integrand simplifies to

$$K\sqrt{g_{\rm opt}} \approx \frac{r_s}{r^2} + \frac{2\pi\rho_0 r_0^3(r_0 - 3r)}{r^3(r + r_0)}. \tag{50}$$

Upon performing the integration, the weak-field deflection angle is found to be

$$\alpha \approx \frac{2r_s}{b} + \frac{4\pi\rho_0 r_0^3}{b}. \tag{51}$$

In the absence of dark matter ($\rho_0 = 0$), the above expression reduces to

$$\alpha = \frac{2r_s}{b}, \tag{52}$$

which is precisely the standard Schwarzschild weak deflection angle [31].

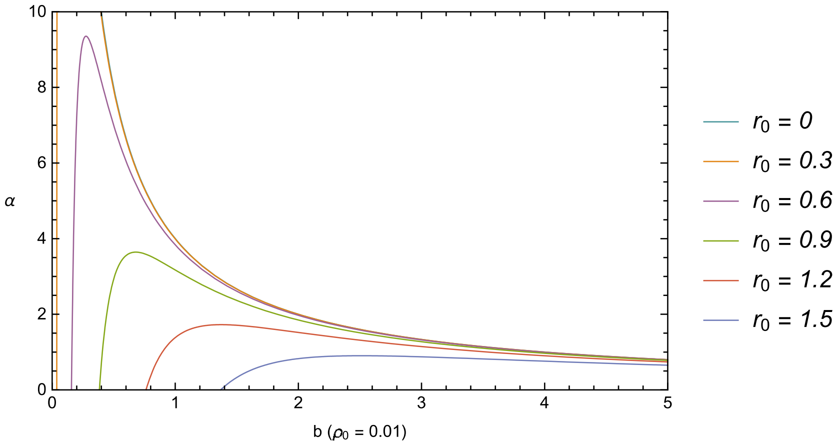

Fig. 4. (color online) Variation of the weak deflection angle α as a function of the impact parameter b for various values of r_0 and fixed parameters $r_s = 2$ and $\rho_0 = 0.01$.

Figure 4 illustrates the dependence of the deflection angle α on the impact parameter b for a Schwarzschild black hole embedded in a Hernquist dark matter halo. The black hole mass is fixed at $r_s = 2$ and the dark matter density at $\rho_0 = 0.01$, with different curves corresponding to distinct values of the halo scale radius r_0. As expected, the deflection angle decreases as the impact parameter increases, reflecting the weakening of the gravitational field at larger distances from the compact object. The figure further reveals that larger halo scale radii alter the bending of light and yield observable deviations from the vacuum Schwarzschild case. These deviations arise from the additional gravitational contribution of the surrounding dark matter distribution, indicating that halo environments can imprint measurable signatures on weak gravitational lensing observables.

IV. ORBIT STABILITY AND LYAPUNOV EXPONENT

As demonstrated in the previous section, circular photon orbits in the black hole–dark matter spacetime correspond to extrema of the effective potential. Specifically, the photon sphere is associated with an unstable maximum of this potential, implying that small orbital perturbations amplify over time. The Lyapunov exponent quantifies the rate at which neighboring trajectories diverge, yielding a quantitative measure of orbital instability. Furthermore, within the eikonal regime, this exponent corresponds directly to the imaginary part of black hole quasinormal mode frequencies, thereby linking null geodesics to wave dynamics in curved spacetime.

The dynamics of photons can be conveniently formulated within the Hamiltonian framework. Using the null Lagrangian (24), the Hamiltonian takes the form

$$\begin{aligned} H = \mathcal{L} &= \frac{1}{2}\left[-\frac{E^2}{h(r)} + h(r)p_r^2 + \frac{V_{\rm eff}}{h(r)}\right] \\ &= \frac{1}{2}g^{\mu\nu}p_\mu p_\nu, \end{aligned} \tag{53}$$

where E denotes the conserved photon energy, p_r denotes the radial momentum, and $V_{\rm eff}$ denotes the effective potential associated with angular motion.

For motion restricted to the equatorial plane, the canonical equations become

$$p_r = \frac{\partial \mathcal{L}}{\partial \dot{r}} = \frac{\dot{r}}{h(r)}, \qquad \dot{r} = \frac{\partial H}{\partial p_r} = h(r)p_r, \tag{54}$$

$$\begin{aligned} \dot{p}_r = -\frac{\partial H}{\partial r} = -\frac{1}{2}\Bigg[& h'(r)p_r^2 + \frac{V'_{\rm eff}(r)}{h(r)} \\ & -\frac{h'(r)}{h^2(r)}\left(-E^2 + V_{\rm eff}(r)\right)\Bigg]. \end{aligned} \tag{55}$$

For a circular photon orbit at $r = r_c$, the conditions

$$V_{\rm eff}(r_c) = E^2, \qquad V'_{\rm eff}(r_c) = 0, \tag{56}$$

hold identically. Expanding about the circular orbit by introducing small perturbations

$$r = r_c + \delta r, \qquad p_r = \delta p_r, \tag{57}$$

and, when only linear contributions are retained, the equations of motion reduce to

$$\delta\dot{r} = h(r_c)\delta p_r, \tag{58}$$

$$\delta\dot{p}_r = -\frac{1}{2}\frac{V''_{\rm eff}(r_c)}{h(r_c)}\delta r. \tag{59}$$

The perturbation dynamics can therefore be expressed in matrix form as

$$\frac{\mathrm{d}}{\mathrm{d}\lambda}\begin{pmatrix}\delta r\\ \delta p_r\end{pmatrix}=\begin{pmatrix}0 & h(r_c)\\ -\dfrac{1}{2}\dfrac{V_{\mathrm{eff}''}(r_c)}{h(r_c)} & 0\end{pmatrix}\begin{pmatrix}\delta r\\ \delta p_r\end{pmatrix},\tag{60}$$

where λ denotes the affine parameter along the null geodesic.

The Lyapunov exponent Λ is determined by the eigenvalues of the stability matrix, which satisfy

$$\left|\begin{pmatrix}0 & h(r_c)\\ -\dfrac{1}{2}\dfrac{V_{\mathrm{eff}''}(r_c)}{h(r_c)} & 0\end{pmatrix}-\Lambda I\right|=0.\tag{61}$$

Solving the characteristic equation yields

$$\begin{aligned}\Lambda^2&=-\frac{V''_{\mathrm{eff}}(r_c)}{2}=-\frac{L^2}{2}\frac{\mathrm{d}^2}{\mathrm{d}r_c^2}\left(\frac{h(r_c)}{r_c^2}\right)\\&=L^2\left[-\frac{h''(r_c)}{2r_c^2}+\frac{2h'(r_c)}{r_c^3}-\frac{3h(r_c)}{r_c^4}\right].\end{aligned}\tag{62}$$

The sign of $V''_{\mathrm{eff}}(r_c)$ determines the stability of the circular orbit. When $V''_{\mathrm{eff}}(r_c)>0$, the Lyapunov exponent becomes imaginary, and the orbit is stable under small perturbations. Conversely, when $V''_{\mathrm{eff}}(r_c)<0$, the Lyapunov exponent is real, and the orbit is unstable; this implies that nearby photon trajectories diverge exponentially over time. Under these conditions, photons initially near the circular orbit eventually either escape to infinity or plunge into the black hole. The magnitude of Λ thus characterizes the instability timescale of the photon sphere and provides crucial insight into the dynamical structure of the spacetime.

Figure 5 depicts the dependence of Λ^2 on the circular orbit radius for various values of the halo scale radius r_0, at a fixed dark matter density $\rho_0=0.01$. The Hernquist dark matter halo significantly alters the stability properties of photon orbits relative to the vacuum Schwarzschild geometry. Specifically, increasing the halo scale radius shifts the region where $\Lambda^2<0$, thereby enlarging the domain of orbital stability. These results demonstrate that extended dark matter distributions can partially stabilize photon motion and modify the dynamical properties of null geodesics near the black hole.

V. SCALAR QUASINORMAL MODES

Quasinormal modes represent the characteristic damped oscillations induced by perturbations of a black hole spacetime. These oscillations encode crucial information regarding the geometry and stability of the underlying spacetime and are characterized by complex frequencies. The real part of the frequency determines the oscillation rate, while the imaginary part governs the damping timescale of the perturbation. In black hole physics, quasinormal modes play a pivotal role in gravitational-wave phenomenology and provide a direct probe of the near-horizon geometry.

In this work, we consider scalar perturbations propagating in the spacetime of a Schwarzschild black hole surrounded by a Hernquist dark matter halo. The dynamics of the scalar field are governed by the covariant Klein–Gordon equation,

$$\left[\frac{1}{\sqrt{-g}}\partial_\mu\left(\sqrt{-g}\,g^{\mu\nu}\partial_\nu\right)-m^2\right]\psi=0,\tag{63}$$

where m denotes the mass of the scalar field and g is the determinant of the spacetime metric.

Exploiting the spherical symmetry of the geometry, we adopt the separable ansatz

$$\psi(t,r,\theta,\phi)=\mathrm{e}^{-\mathrm{i}\omega t}R(r)Y_l^{m_l}(\theta,\phi),\tag{64}$$

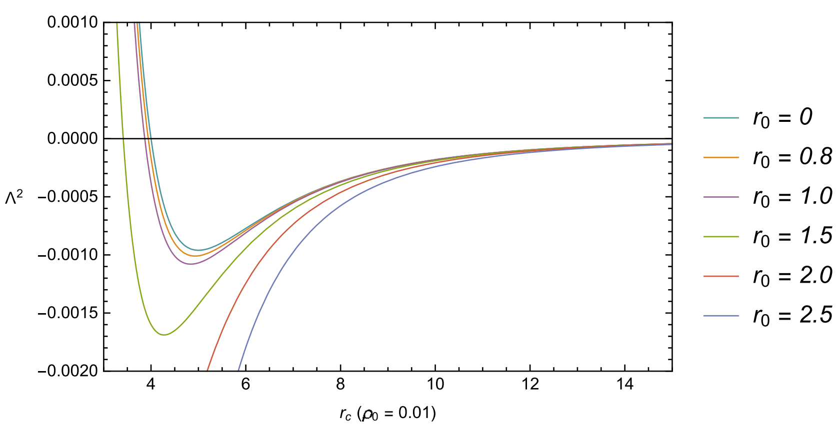

Fig. 5. (color online) Profile of Λ^2 as a function of the circular orbit radius for various values of the Hernquist halo parameters.

where $Y_l^{m_l}(\theta,\phi)$ are the standard spherical harmonics. Substituting this decomposition into the Klein–Gordon equation reduces the problem to a radial differential equation,

$$\partial_r\left(h(r)r^2\partial_r R(r)\right)+\left[\omega^2\frac{r^2}{h(r)}-l(l+1)-m^2r^2\right]R(r)=0. \quad (65)$$

To analyze the quasinormal spectrum, we consider the massless case and introduce the tortoise coordinate r^*, defined by

$$\mathrm{d}r^*=\frac{\mathrm{d}r}{h(r)}, \quad (66)$$

together with the field redefinition

$$R(r)=\frac{\mathcal{R}(r^*)}{r}. \quad (67)$$

Under these transformations, Eq. (65) assumes the Schrödinger-like form

$$\frac{\mathrm{d}^2\mathcal{R}(r^*)}{\mathrm{d}r^{*2}}+\left[\omega^2-V(r)\right]\mathcal{R}(r^*)=0, \quad (68)$$

with the effective potential

$$V(r)=\frac{h(r)}{r^2}\left[l(l+1)+rh'(r)\right]. \quad (69)$$

The effective potential forms a barrier outside the black hole horizon, and quasinormal modes correspond to waves that are purely ingoing at the horizon and purely outgoing at spatial infinity. In the eikonal regime, where the multipole number satisfies $l\gg 1$, the dominant contribution to the potential becomes

$$V(r)\approx\frac{l^2h(r)}{r^2}. \quad (70)$$

Consequently, the radial equation reduces to

$$\frac{\mathrm{d}^2\mathcal{R}(r^*)}{\mathrm{d}r^{*2}}+W(r)\mathcal{R}(r^*)=0, \quad (71)$$

$$W(r)=\omega^2-\frac{l^2}{L^2}V_{\text{eff}}(r), \quad (72)$$

revealing a direct correspondence between scalar quasinormal modes and the effective potential governing null geodesics.

In this high-frequency limit, the quasinormal spectrum can be obtained using the WKB approximation developed by Schutz, Iyer, and Will [35]. The WKB quantization condition is given by

$$\frac{W(r_0)}{\sqrt{2W^{(2)}(r_0)}}=-\mathrm{i}\left(n+\frac{1}{2}\right), \quad (73)$$

where n is the overtone number and

$$W^{(2)}(r_0)=\left.\frac{\mathrm{d}^2W}{\mathrm{d}r^{*2}}\right|_{r=r_0}. \quad (74)$$

The point r_0 corresponds to the maximum of the effective potential and coincides with the radius of the unstable circular null orbit, *i.e.*, $r_0=r_c$. Evaluating the WKB condition at this maximum yields

$$\omega_{\text{QNM}}\approx\frac{l}{|L|}\sqrt{V_{\text{eff}}(r_c)}-\mathrm{i}\left(n+\frac{1}{2}\right)\sqrt{-\frac{1}{2V_{\text{eff}}(r_c)}\left.\frac{\mathrm{d}^2V_{\text{eff}}}{\mathrm{d}r^{*2}}\right|_{r=r_c}}. \quad (75)$$

Using

$$\left.\frac{\mathrm{d}^2V_{\text{eff}}}{\mathrm{d}r^{*2}}\right|_{r=r_c}=h^2(r_c)V''_{\text{eff}}(r_c). \quad (76)$$

The quasinormal frequencies can be expressed directly in terms of the Lyapunov exponent derived in the preceding section

$$\omega_{\text{QNM}}=\frac{l}{|L|}\sqrt{V_{\text{eff}}(r_c)}-\mathrm{i}\left(n+\frac{1}{2}\right)\frac{|\Lambda|}{L^2}r_c^2\sqrt{V_{\text{eff}}(r_c)}. \quad (77)$$

This relation establishes a striking geometric correspondence between the quasinormal spectrum and the properties of unstable photon orbits. The real part of the frequency is determined by the angular velocity of photons orbiting the photon sphere, whereas the imaginary part is governed by the Lyapunov exponent, which quantifies the orbital instability timescale. Consequently, the quasinormal ringing of the black hole is intrinsically linked to the dynamics of null geodesics near the photon sphere.

In the weak dark matter regime, $\rho_0r_0^4\ll 1$, a perturbative expansion yields

$$\begin{aligned}\omega_{\text{QNM}}=&\frac{2l}{3\sqrt{3}r_s^2}\left[1+\frac{16\pi\rho_0r_0^4}{3r_s^2}\right]\\&-\mathrm{i}\frac{2n+1}{3\sqrt{3}r_s^2}\left[r_s+\frac{16\pi\rho_0r_0^4}{9r_s}\right].\end{aligned} \quad (78)$$

In the absence of dark matter, the effective potential reduces to the standard Schwarzschild form,

$$V_{\rm eff}(r) = \frac{L^2}{r^2}\left(1-\frac{2M}{r}\right), \tag{79}$$

for which the unstable circular null orbit lies at $r_c = 3M$. We then obtain

$$\Lambda = \frac{|L|}{9M^2}, \qquad V_{\rm eff}(r_c) = \frac{L^2}{27M^2}, \tag{80}$$

leading to the established Schwarzschild quasinormal frequencies [36],

$$\omega_{\rm QNM}^{\rm Schwarzschild} = \frac{l}{3\sqrt{3}M} - \frac{{\rm i}\left(n+\dfrac{1}{2}\right)}{3\sqrt{3}M}. \tag{81}$$

VI. THERMODYNAMICS

We now consider the thermodynamic properties of the Schwarzschild black hole immersed in a Hernquist dark matter halo. The surrounding dark matter distribution modifies the horizon structure, thereby altering the thermal behavior of the black hole spacetime. Specifically, the halo introduces nontrivial corrections to the Hawking temperature, heat capacity, and Gibbs free energy, resulting in thermodynamic features absent from the vacuum Schwarzschild geometry.

The event horizon radius r_H is determined from the condition

$$g_{tt}(r_H) = h(r_H) = 0, \tag{82}$$

which gives the black hole mass

$$M = \frac{r_H}{2} + \frac{2\pi\rho_0 r_0^3 r_H}{r_0 + r_H}. \tag{83}$$

Within the framework of black hole chemistry, the mass parameter is interpreted as the thermodynamic enthalpy of the system [37, 38]. The Hawking temperature follows from the surface gravity evaluated at the event horizon,

$$T = \frac{h'(r_H)}{4\pi} = \frac{1}{4\pi r_H} - \frac{\rho_0 r_0^4}{2(r_0+r_H)^2}. \tag{84}$$

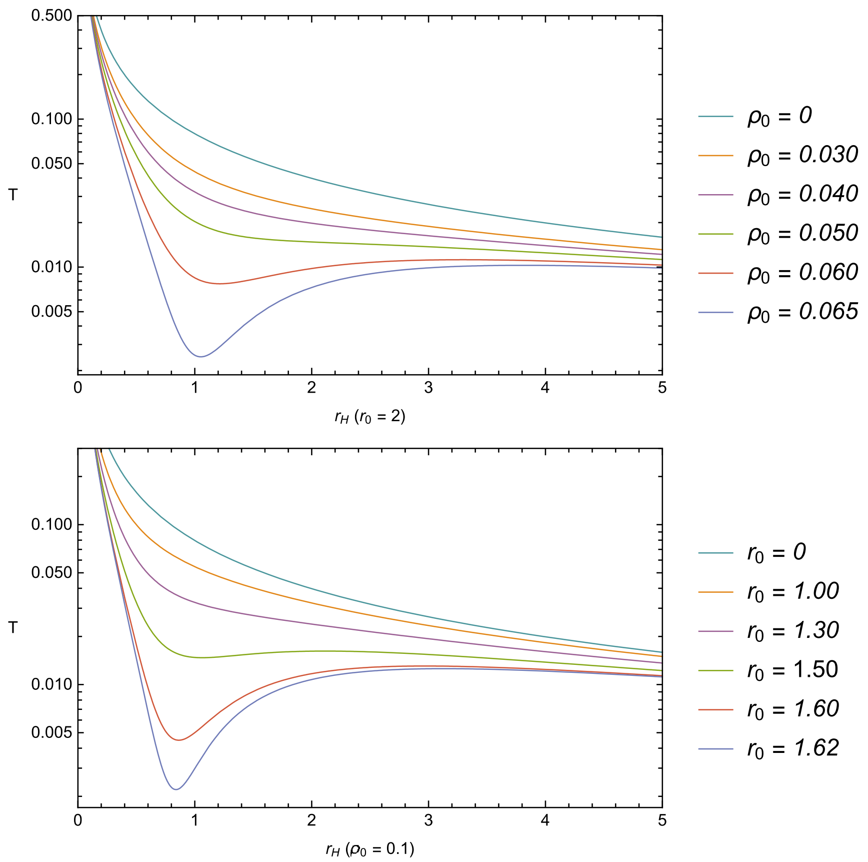

Fig. 6. (color online) Temperature T as a function of the horizon radius r_H for different values of the Hernquist halo parameters $\{\rho_0, r_0\}$.

Figure 6 illustrates the Hawking temperature as a function of the horizon radius for various values of the halo parameters $\{\rho_0, r_0\}$. In the upper panel, the halo scale radius is fixed at $r_0 = 2$ and the dark matter density ρ_0 is varied; in the lower panel, $\rho_0 = 0.1$ is fixed while the halo scale radius is varied. Compared with the Schwarzschild case, the dark matter halo significantly modifies the thermal profile, producing extrema in the temperature curve for sufficiently large halo parameters. These extrema indicate the emergence of nontrivial thermodynamic phases.

The black hole entropy can be derived from the first law of thermodynamics,

$$S = \int \frac{1}{T}\frac{\mathrm{d}M}{\mathrm{d}r_H} dr_H = \pi r_H^2 = \frac{A}{4}, \tag{85}$$

which reproduces the standard Bekenstein–Hawking area law. The entropy remains positive and continuous for all physically admissible values of the horizon radius, indicating that the dark matter halo preserves the fundamental geometric nature of black hole entropy.

To investigate the local thermodynamic stability of the system, we compute the heat capacity,

$$C_H = \frac{\partial M}{\partial T} = \frac{\dfrac{\partial M}{\partial r_H}}{\dfrac{\partial T}{\partial r_H}} = \frac{2\pi r_H^2 (r_0 + r_H)^2 \left[(r_0 + r_H)^2 + 2\pi\rho_0 r_0^4\right]}{(r_0 + r_H)^3 - 4\pi\rho_0 r_0^4 r_H^2}. \tag{86}$$

The variation of the heat capacity is illustrated in Fig. 7. For a Schwarzschild black hole (corresponding to $\rho_0 = 0$), the heat capacity is always negative, reflecting the well-known thermodynamic instability of asymptotically flat black holes [39]. The inclusion of the Hernquist dark matter halo substantially modifies this scenario, producing regions where $C_H > 0$ that correspond to thermodynamically stable black hole phases. Increasing either the dark matter density ρ_0 or the halo scale radius r_0 expands the stable region and shifts the divergence points of the heat capacity.

The divergences of C_H occur at

$$\frac{\partial T}{\partial r_H} = 0, \tag{87}$$

which correspond to extrema of the temperature curve. Regions where $T(r_H)$ exhibits a positive slope are associated with a positive heat capacity and thus local stability,

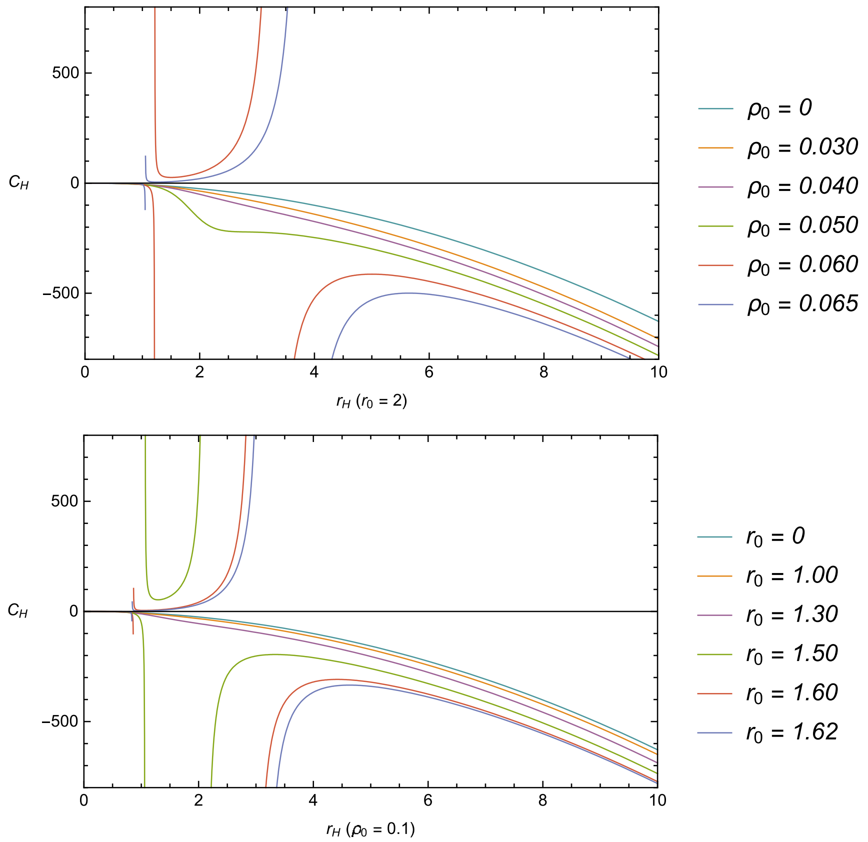

Fig. 7. (color online) The heat capacity C_H as a function of the horizon radius r_H for various values of the Hernquist halo parameters $\{\rho_0, r_0\}$.

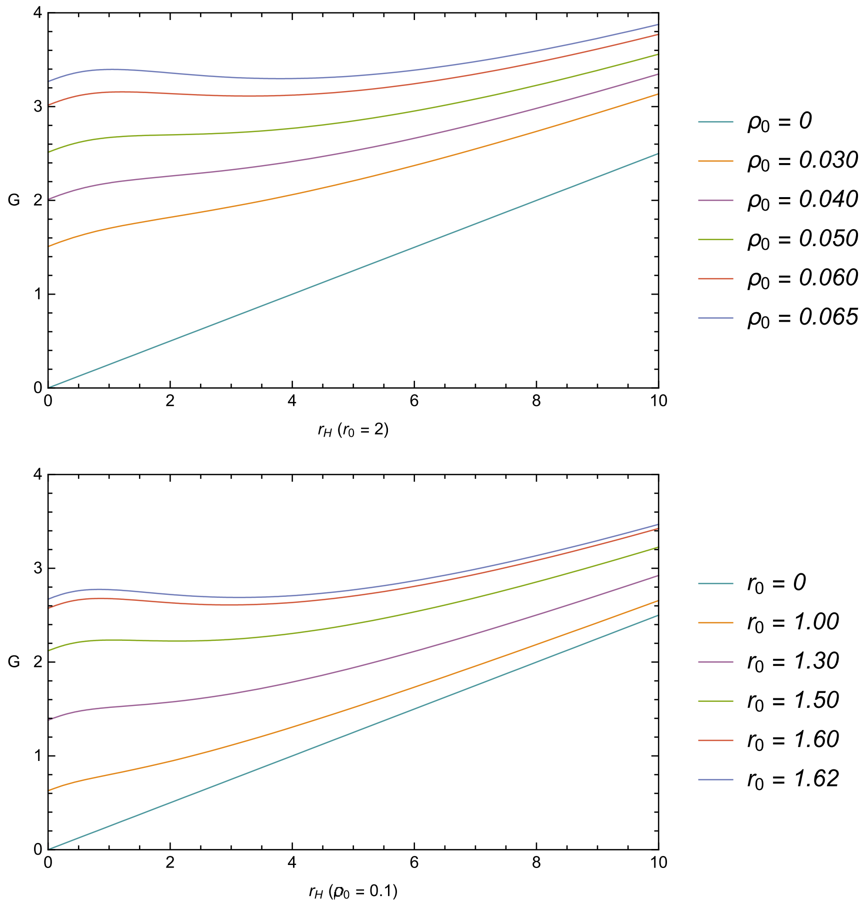

Fig. 8. (color online) The Gibbs free energy G as a function of the horizon radius r_H for different values of the Hernquist halo parameters $\{\rho_0, r_0\}$.

whereas negative slopes indicate unstable thermodynamic branches. For a sufficiently small dark matter density, the temperature exhibits no extrema, and no stable phase emerges.

To analyze the global thermodynamic structure of the black hole–halo system, we evaluate the Gibbs free energy,

$$G = M - TS = \frac{r_H}{4} + \frac{\pi\rho_0 r_0^4(r_0+2r_H)}{(r_0+r_H)^2}. \tag{88}$$

Figure 8 presents the Gibbs free energy as a function of the horizon radius for various halo configurations. The upper panel corresponds to a fixed $r_0 = 2$ and varying ρ_0, whereas the lower panel corresponds to a fixed $\rho_0 = 0.1$ and varying r_0. The dark matter halo significantly modifies the global thermodynamic behavior of the spacetime, expanding the region of positive Gibbs free energy and thereby indicating an increase in globally unstable configurations.

Figure 9 illustrates the thermodynamic profiles of the Gibbs free energy, entropy, and heat capacity as functions of temperature for a fixed halo radius of $r_0 = 2$. The critical points are determined from the conditions

$$\frac{\partial G}{\partial T} = \frac{\partial^2 G}{\partial T^2} = 0. \tag{89}$$

At the critical temperature, the Gibbs free energy and its first derivative remain continuous, whereas the second derivative becomes singular. This singularity manifests as a divergence in the heat capacity, indicating an infinite thermodynamic response to infinitesimal temperature variations. In contrast, the entropy remains continuous throughout the transition.

The phase transition occurs at the inflection point of the entropy curve, where

$$\frac{\partial S}{\partial T} \to \infty, \tag{90}$$

and vanishes in the absence of such an inflection point. Although the Gibbs free energy may develop swallowtail-like structures for certain halo parameters, the continuity of the entropy precludes latent heat, thereby ruling out a first-order phase transition. Instead, the divergence of the

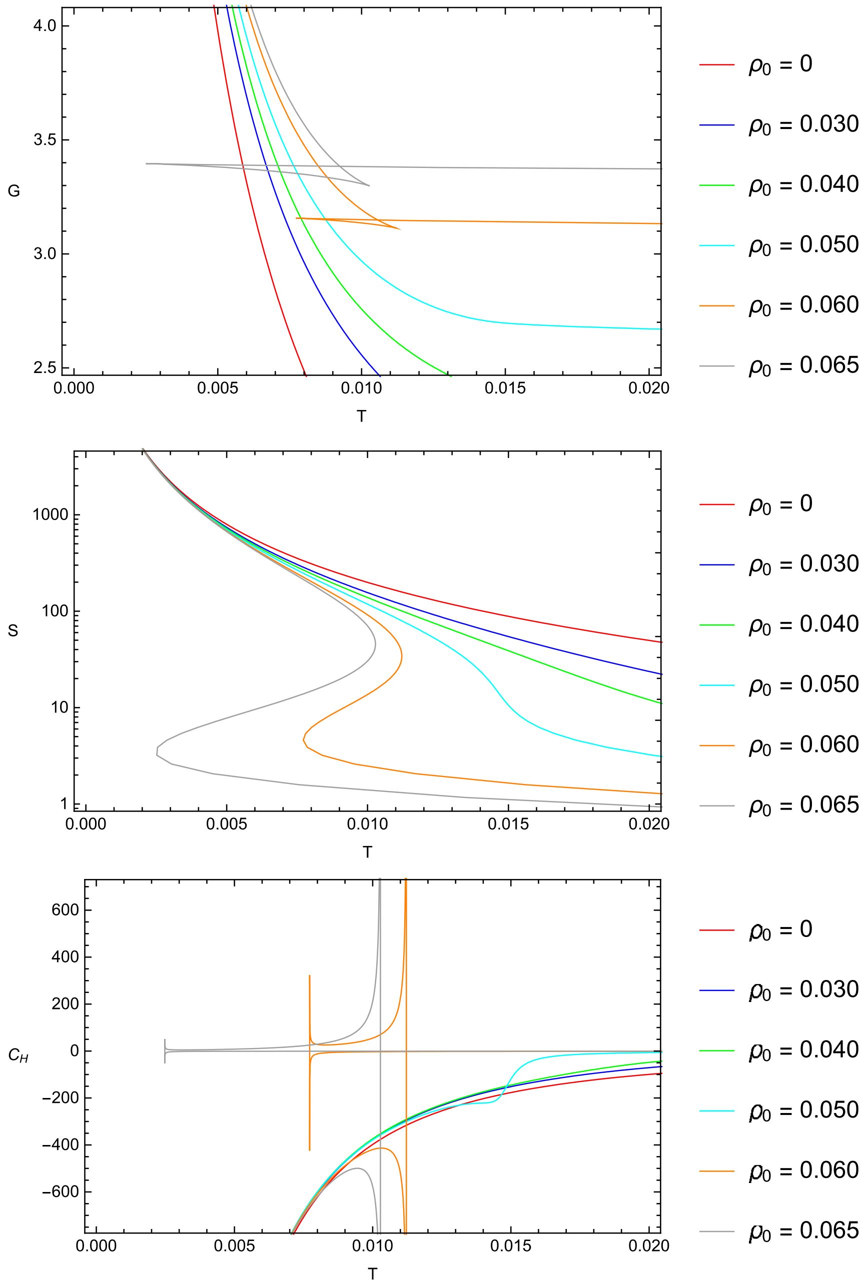

Fig. 9. (color online) Profiles of the Gibbs free energy $G(T)$, entropy $S(T)$, and heat capacity $C_H(T)$ for various values of the Hernquist halo parameters, with $r_0 = 2$ held fixed.

heat capacity indicates a second-order phase transition within the Ehrenfest classification, wherein first derivatives of the Gibbs free energy remain continuous whereas second derivatives become singular. In the Schwarzschild limit $\rho_0 = 0$, no such transition occurs, consistent with the standard thermodynamic behavior of vacuum black holes.

VII. SUMMARY

In this work, we constructed an exact, static, spherically symmetric black hole solution immersed in a Hernquist dark matter halo by directly solving the Einstein field equations. Unlike previous treatments in which the metric fails to consistently reproduce the prescribed matter distribution at the level of the Einstein tensor, our construction ensures full compatibility between the spacetime geometry and the underlying dark matter source. This yields a self-consistent gravitational realization of a black hole embedded in a Hernquist halo, enabling a systematic investigation of its optical, dynamical, and thermodynamic properties.

We first examined photon propagation in the black hole–halo spacetime by analyzing null geodesics and their associated effective potential. The surrounding dark matter distribution modifies photon trajectories and shifts the circular null orbit away from its Schwarzschild value. As the halo parameters ρ_0 and r_0 increase, both the photon sphere radius and the critical impact parameter decrease, resulting in a smaller apparent shadow radius. The weak deflection angle is similarly affected by the halo environment; light bending weakens for more extended dark matter distributions. These results demonstrate that dark matter can imprint observable signatures on gravitational lensing phenomena and black hole shadow structures.

We further investigated the stability of circular photon orbits by deriving the Lyapunov exponent for radial perturbations. Because unstable null geodesics govern the eikonal behavior of quasinormal modes, this analysis establishes a direct connection between the photon sphere's geometric structure and the spacetime's dynamical response to perturbations. In the eikonal regime, we showed that quasinormal mode frequencies acquire explicit corrections induced by the dark matter halo. For dilute halo configurations, increasing either ρ_0 or r_0 enhances both the real and imaginary parts of the quasinormal frequencies, indicating higher oscillation frequencies and faster perturbation damping.

We then explored the thermodynamic properties of the black hole–halo system via the Hawking temperature, entropy, heat capacity, and Gibbs free energy. The entropy continues to satisfy the standard Bekenstein–Hawking area law, remaining positive and continuous across the physical parameter range. In contrast, the dark matter environment strongly modifies the temperature profile, which may develop extrema absent in the Schwarzschild case. These extrema generate heat capacity divergences, signaling transitions between thermodynamically stable and unstable branches. While the Schwarzschild black hole possesses negative heat capacity for all horizon radii, including the Hernquist halo introduces regions of positive heat capacity, thereby enlarging the domain of local thermodynamic stability.

We analyzed the global thermodynamic structure via the Gibbs free energy. Increasing the halo density or scale radius enlarges the region where the Gibbs free energy is positive, indicating enhanced global instability of the black hole configuration. By examining the behavior of $G(T)$, $S(T)$, and $C_H(T)$, we identified critical points characterized by heat capacity divergences alongside continuous Gibbs free energy and entropy. This behavior indicates a second-order phase transition within the Ehrenfest classification. Although swallow-tail-like structures may emerge in the Gibbs free energy for certain halo parameters, the continuity of the entropy excludes latent heat, thereby ruling out a first-order transition. In the limit $\rho_0 \to 0$, all results smoothly reduce to those of the standard Schwarzschild black hole.

Overall, our analysis demonstrates that realistic dark matter environments can substantially modify both the optical and thermodynamic behavior of black holes. The Hernquist halo not only alters photon motion and quasinormal spectra but also generates nontrivial thermodynamic phases absent in vacuum geometries. These effects may yield potentially observable signatures of halo-induced gravitational physics and offer new insights into the interplay between black holes, dark matter, and galactic environments.

References

[1] M. M. Gohain, P. Phukon, and K. Bhuyan, Phys. Dark Univ. **46**, 101683 (2024), arXiv: 2407.02872[gr-qc]

[2] D. Senjaya, Eur. Phys. J. C **85**(11), 1256 (2025). [Erratum: Eur. Phys. J. C **86**, 37 (2026)]

[3] B. Toshmatov, B. Ahmedov, A. Boydedayev *et al*., Phys. Rev. D **111**(12), 124058 (2025)

[4] D. Senjaya, T. Chuensuksan, and S. Ponglertsakul, (2026), arXiv: 2602.03349 [gr-qc]

[5] U. Uktamov, S. Shaymatov, B. Ahmedov, (2025), arXiv: 2505.20031 [gr-qc]

[6] D. Senjaya, Eur. Phys. J. C **86**(5), 528 (2026)

[7] A. Al-Badawi, S. Shaymatov, and Y. Sekhmani, JCAP **02**, 014 (2025), arXiv: 2411.01145[gr-qc]

[8] B. P. Abbott *et al*., Phys. Rev. Lett. **116**(24), 241102 (2016), arXiv: 1602.03840[gr-qc]

[9] K. Akiyama *et al*., Astrophys. J. Lett. **875**(1), 6 (2019), arXiv: 1906.11243

[10] S. Rani, A. Jawad, M. Heydari-Fard *et al*., Eur. Phys. J. C **85**(6), 677 (2025)

[11] H. Zhao, Mon. Not. Roy. Astron. Soc. **278**, 488 (1996)

[12] W. Dehnen, Mon. Not. Roy. Astron. Soc. **265**, 250 (1993)

[13] D. Senjaya and P. Sereewat, Phys. Dark Univ. **52**, 102264 (2026)

[14] D. Senjaya, Eur. Phys. J. C **86**, 161 (2026)

[15] A. Benkrane, Phys. Dark Univ. **50**, 102130 (2025)

[16] A. R. P. Moreira, A. Bouzenada, F. M. Belchior *et al*., (2026), arXiv: 2605.24046

[17] Z. Xu, X. Hou, X. Gong *et al*., JCAP **09**, 038 (2018), arXiv: 1803.00767[gr-qc]

[18] S. Jumaniyozov, J. Rayimbaev, O. Sirajiddin *et al*., Nucl. Phys. B **1025**, 117404 (2026)

[19] S. Qi and Z. Cai, Eur. Phys. J. C **86**(1), 94 (2026)

[20] S. W. Hawking, Phys. Rev. D **13**, 191 (1976)

[21] W. Israel, Phys. Rev. **164**, 1776 (1967)

[22] B. Carter, Phys. Rev. Lett. **26**, 331 (1971)

[23] J. D. Bekenstein, Lett. Nuovo Cim. **4**, 737 (1972)

[24] J. D. Bekenstein, Phys. Rev. D **7**, 2333 (1973)

[25] R. N. Izmailov, E. R. Zhdanov, A. Bhadra *et al*., Eur. Phys. J. C **79**(2), 105 (2019)

[26] R. B. Mann, JHAP **4**(1), 1 (2024), arXiv: 2403.02864[hep-th]

[27] R. B. Mann, Int. J. Mod. Phys. D **34**(09), 2542001 (2025)

[28] R. C. Pantig, Phys. Dark Univ. **45**, 101550 (2024), arXiv: 2405.07531[gr-qc]
[29] V. Perlick and O. Y. Tsupko, Phys. Rept. **947**, 1 (2022), arXiv: 2105.07101[gr-qc]
[30] G. W. Gibbons and M. C. Werner, Class. Quant. Grav. **25**, 235009 (2008), arXiv: 0807.0854[gr-qc]
[31] H. Waseem, N. J. L. S. Lobos, A. Övgün *et al*., Eur. Phys. J. C **85**(6), 629 (2025), arXiv: 2502.04044[gr-qc]
[32] F. Ahmed, İ. Sakallı, and A. Al-Badawi, Phys. Lett. B **864**, 139448 (2025), arXiv: 2503.00082[gr-qc]
[33] E. Sucu and İ. Sakallı, Phys. Rev. D **111**(6), 064049 (2025)
[34] S. Mandal, Phys. Dark Univ. **42**, 101374 (2023), arXiv: 2309.16461[gr-qc]
[35] B. F. Schutz and C. M. Will, Astrophys. J. Lett. **291**, 33 (1985)
[36] V. Ferrari and B. Mashhoon, Phys. Rev. D **30**, 295 (1984)
[37] D. Kastor, S. Ray, and J. Traschen, Class. Quant. Grav. **26**, 195011 (2009), arXiv: 0904.2765[hep-th]
[38] D. Kastor, S. Ray, and J. Traschen, Class. Quant. Grav. **36**(2), 024002 (2019), arXiv: 1807.09801[gr-qc]
[39] A. Benkrane and D. E. Zenkhri, Nucl. Phys. B **1018**, 117069 (2025)